

Experimental and numerical analyses of electrohydrodynamic force according to air pressure

Rong-Hui Quan(全荣辉), Bo Wang(王博), and Yun-Jia Yao(姚韵佳)
Citation: Chin. Phys. B, 2023, 32 (**6**): 065201. DOI: 10.1088/1674-1056/acac11
Journal homepage: http://cpb.iphy.ac.cn; http://iopscience.iop.org/cpb

What follows is a list of articles you may be interested in

Fractal microstructure of Ag film via plasma discharge as SERS substrates

Xue-Fen Kan(阚雪芬), Cheng Yin(殷澄), Zhuang-Qi Cao(曹庄琪), Wei Su(苏巍), Ming-Lei Shan(单鸣雷), and Xian-Ping Wang(王贤平)
Chin. Phys. B, 2021, 30 (**12**): 125201. DOI: 10.1088/1674-1056/ac0693

Review on ionization and quenching mechanisms of Trichel pulse

Anbang Sun(孙安邦), Xing Zhang(张幸), Yulin Guo(郭雨林), Yanliang He(何彦良), and Guanjun Zhang(张冠军)
Chin. Phys. B, 2021, 30 (**5**): 055207. DOI: 10.1088/1674-1056/abd75d

Enhancement of corona discharge induced wind generation with carbon nanotube and titanium dioxide decoration

Jianchun Ye(叶建春), Jun Li(李俊), Xiaohong Chen(陈晓红), Sumei Huang(黄素梅), Wei Ou-Yang(欧阳威)
Chin. Phys. B, 2019, 28 (**9**): 095202. DOI: 10.1088/1674-1056/ab33ed

Characteristics and underlying physics of ionic wind in dc corona discharge under different polarities

Tongkai Zhang(张桐恺), Yu Zhang(张宇), Qizheng Ji(季启政), Ben Li(李犇), Jiting Ouyang(欧阳吉庭)
Chin. Phys. B, 2019, 28 (**7**): 075202. DOI: 10.1088/1674-1056/28/7/075202

Using a Mach–Zehnder interferometer to deduce nitrogen density mapping

F. Boudaoud, M. Lemerini
Chin. Phys. B, 2015, 24 (**7**): 075205. DOI: 10.1088/1674-1056/24/7/075205

Experimental and numerical analyses of electrohydrodynamic force according to air pressure

Rong-Hui Quan(全荣辉)†, Bo Wang(王博), and Yun-Jia Yao(姚韵佳)

Nanjing University of Aeronautics and Astronautics, College of Astronautics College of Astronautics, Nanjing 211106, *China*

(Received 5 October 2022; revised manuscript received 29 November 2022; accepted manuscript online 16 December 2022)

Electrohydrodynamic (EHD) force produced by corona discharge is considered as a new thrust for solar-powered aircraft and stratosphere balloons in near space. However, its performance at low air pressures remains to be clarified. An experiment of measuring the EHD force at 0.02 atm–1.0 atm (1 atm = 1.01325×10^5 Pa) is carried out with the wire-to-cylinder geometric structure. The ion distribution is analyzed by using the drift-diffusion model with two-dimensional numerical simulation. The experimental result shows that the EHD force is not linearly related to the corona discharge current at low air pressures. Numerical simulation finds that the proportion of ions in the counter-direction electric field increases from approximately 0.36% to 30% when the pressure drops from 1.0 atm to 0.2 atm. As a result, the EHD force with a constant power supply drops faster than the previous theoretical prediction in the ground experiment, suggesting that the consideration of counter-direction EHD force is necessary to improve the ionic wind propulsion efficiency in near-space applications.

Keywords: electrohydrodynamic force, ionic wind, corona discharge

PACS: 52.80.–s, 52.80.Hc, 51.10.+y, 52.40.Kh **DOI:** 10.1088/1674-1056/acac11

1. Introduction

Electrohydrodynamic (EHD) force is produced by corona discharges when ions are accelerated by the electric field and transfer their momenta to neutral air molecules.[1] It is usually achieved in the discharging structure of dielectric barriers or wire-to-cylinder electrodes. The EHD force has diverse applications, such as providing thrust for the electrostatic precipitator or air vehicles.[2–8] Comparing with conventional propellers or turbofans, the generation of EHD force requires neither mechanical components nor chemical combustion, and it is nearly silent. With the development of material and electrical technology, EHD force has received attention in recent years.[9–11] Both experimental and theoretical results show that EHD force has a high thrust-to-power ratio but low thrust-to-area density at atmospheric pressure (in unit atm). However, when EHD force is used to maintain the position of stratosphere balloons or drive solar-powered aircraft, as studied in Ref. [12], its performance at high altitude is still unclear,[13–15] as most of studies were conducted at atmospheric pressure on the ground.

In 2018, Gilmore and Barrett theoretically analyzed the effects of altitude and flight speed on EHD force and predicted that the EHD force decreases with flight altitude increasing at a constant power consumption.[16] In 2021, Khomich *et al.* measured the EHD force at pressures from 1.0 atm down to 0.05 atm during positive corona discharge.[17] The experimental results confirmed the decrease in EHD force with air pressure lowering. However, the predictions obtained in Ref. [16] do not fit the experimental results well. In theoretical prediction, a 75% decline in the thrust-to-power ratio occurs at 20-km altitude, but it shows a 98% drop in Ref. [17]. The reason for such an inconsistency is still unclear. Here, we carry out the experiment at different pressures and use the drift-diffusion model to analyze the air pressure effect on EHD force,[18,19] in order to better understand the EHD force at high altitudes.

2. Experiment setup

A vacuum chamber is convenient for conducting experiments at low air pressure. Thus, we used a vacuum chamber with a length of 1.5 m and a diameter of 2.0 m for the experiment. The chamber was of stainless steel and electrically grounded to keep the internal electric field undisturbed. An adjustable vent valve was used to control the inflow airspeed for pressure balance inside the chamber. We varied the air pressure from 1.0 atm to 10^{-3} atm with an accuracy of 1.5%.

The EHD cell had three parallel sets of anodes and cathodes (Fig. 1), and each element was 40 cm in length. The anodes were positively biased. They were made of tungsten and had a diameter of 50 μm. The metal rod cathodes, each with a diameter of 10 mm, were grounded. The distance between each discharging set was 14.5 cm, and the gap between the anode and cathode was adjustable from 2.0 cm to 14 cm. The chassis was made of high-resistivity Teflon.

Figure 2 shows the schematic diagram of the experimental setup. It consisted of a vacuum system, EHD cell, high-voltage power supply, and measurement system. The Glassman EJ20P30 power supply controlled the bias voltage on the anode. The voltage was increased from 0 kV up to the inception voltage to trigger off the corona discharge. Then it

†Corresponding author. E-mail: quanrh@nuaa.edu.cn

© 2023 Chinese Physical Society and IOP Publishing Ltd

was slowly increased up to the power supply limit or the cell breakdown voltage at low air pressures.

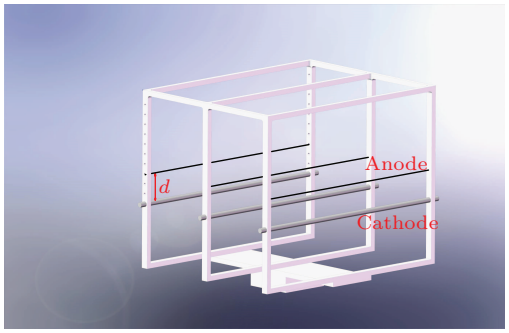


Fig. 1. Structure of EHD cell.

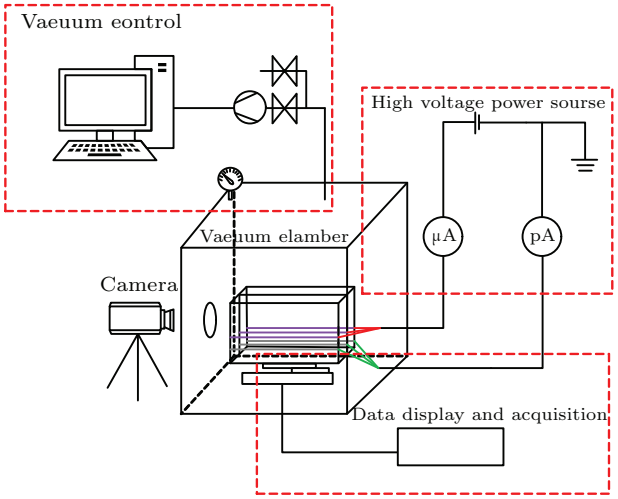


Fig. 2. Schematic diagram of experiment setup.

The measurement system contained a force measurement load cell and two current meters. The EHD cell was mounted on an insulation plate above the load cell at a height of 5.0 cm. A high-resolution SBT431 load cell with a resolution of 0.01 g (equivalent to 0.1 mN) was used to measure the EHD force. We used the Keithley 6517B electrometer to measure the current on the cathode with an accuracy of ±10 pA.

During the experiments, the room temperature was 25 ± 1 °C. The electrode gap distance was fixed at 20 mm, 60 mm, 100 mm, and 140 mm separately. The vent valve adjusted the air pressure balance inside the chamber. Once the desired pressure was achieved and stable, the high-voltage power supply delivered bias voltage to the anode. The voltage was slowly increased from 0 kV to the feasible maximum. It took at least 15 s to wait for the corona discharge to reach a stable state. The EHD force and discharge current were recorded three times at an interval of 5 min.

3. Experiment results and analyses

3.1. Influence of air pressure on EHD force

Figure 3 shows the EHD force according to the corona discharge current measured at different air pressures. In theory developed by Masuyama and Barrett, the integration form of EHD force is calculated from[7,9]

$$F = \frac{Id}{\mu}, \tag{1}$$

where F is the EHD force, I is the discharge current, μ is the ion mobility, and d is the electrode gap distance. When the gap distance and air pressure are fixed, equation (1) predicts the linear increase in EHD force with the corona discharge current. In Fig. 3, although the thrust increases with the discharge current at different gap distances or air pressures, the growth trend bends as the discharge current increases, breaking the ideal linear relation.

In addition, the EHD force remarkably drops with air pressure increasing. For example, in Fig. 3(a), the thrust force is approximately 38.5 mN when the discharge current is 1.53 mA and the air pressure is 1.0 atm. It drops to 20.6 mN at the same discharge current when the air pressure is 0.5 atm. The result is inconsistent with Khomich's experimental result.[17] However, in Jignesh Soni and Subrata Roy's experiment, the EHD force first increased to a max value and then decreased when the air pressure dropped.[18] The difference may be caused by different EHD cells and bias voltages. In Ref. [18], a dielectric barrier discharge actuator was used and the power was supplied by high-voltage transformer with pulsed voltage output.

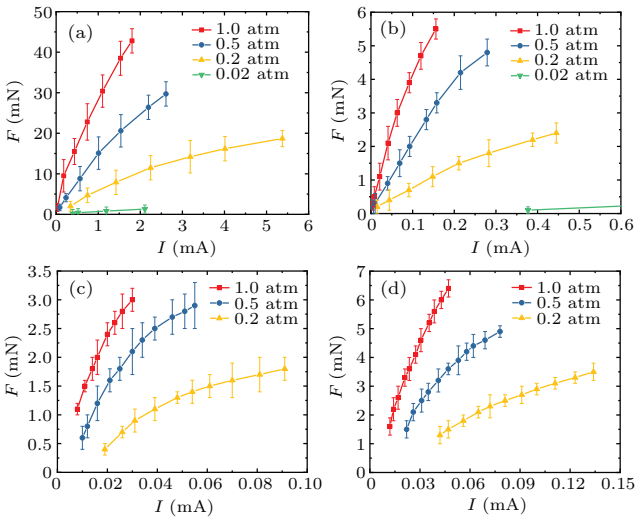


Fig. 3. Measured EHD forces according to discharge current at different air pressures and electrode gap distance d = 20 mm (a), 60 mm (b), 100 mm (c), and 140 mm (d).

The decrease of EHD force with air pressure rising can be explained by the increase of ion mobility with air pressure lowering. The dependence of ion mobility on air pressure splits into two regions. Under low-field limit at a constant temperature, the ion mobility satisfies [16]

$$\mu \propto \frac{1}{P}, \tag{2}$$

where P is the air pressure. When the electric field is strong enough, the ion mobility under the high-field limit (another region) satisfies the following relationship instead:

$$\mu \propto \frac{1}{\sqrt{PE}}, \tag{3}$$

Thus, the ion mobility increases when the air pressure drops. It leads to the decrease of EHD force at lower air pressures as described in Eq. (1). However, it cannot fully explain the break of the linear relation between the EHD force and discharge current.

3.2. Corona discharging current

Corona discharging current determines the number of ions or electrons accelerated in the electric field. When the air pressure drops, the inception voltage of corona discharge is reduced, which leads to the growth of discharging current under the same bias voltage. We measure the corona discharge currents at different air pressures, and the obtained results are shown in Fig. 4.

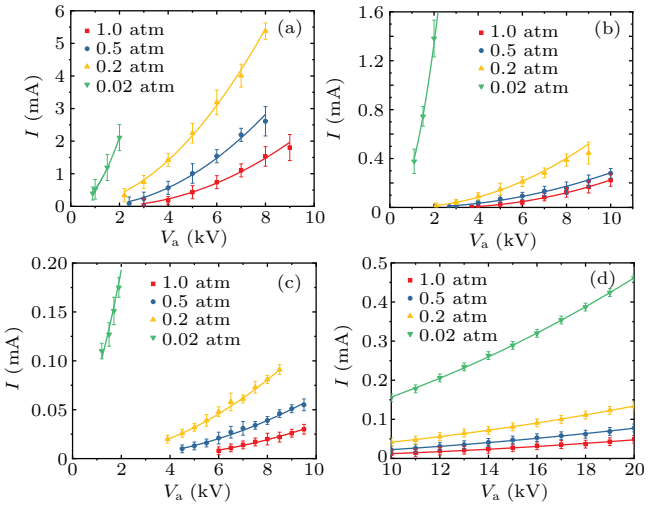


Fig. 4. Measured discharge currents according to bias voltage at different air pressures and electrode gap distances $d = 20$ mm (a), 60 mm (b), 100 mm (c), and 140 mm (d).

Figures 4(a)–4(d) show that the discharge current decreases with the electrode gap distance due to lower mean electric field. When the air pressure drops, ion mobility increases, thereby increasing the corona discharge current. The dependence of discharging current on bias voltage can be written as[17]

$$I = A\frac{9}{8}\mu\varepsilon_0\frac{(V_a - V_c)^2}{d^3}, \tag{4}$$

where I is the discharging current, A is the cross-section area of the drift region, ε_0 is the electric constant, V_a is the bias voltage on the anode, and V_c is the inception voltage. The inception voltage decreases with the air pressure rising and increases with the electrode gap distance increasing. For example, V_c is 2.9 kV at a pressure of 1.0 atm and drops to 0.9 kV at 0.02 atm for the same gap distance $d = 20$ mm. By substituting Eq. (4) into Eq. (1), we obtain

$$F = A\frac{9\varepsilon_0}{8}\frac{(V_a - V_c)^2}{d^2}. \tag{5}$$

Equation (5) implies that the EHD force is insensitive to ion mobility and only related to the difference between bias voltage and inception voltage, the electrode gap distance and the drift cross-section area. If drift cross-section A is constant, by moving other variables to the left-hand side of Eq. (5), we obtain the following expression:

$$\frac{F}{(V_a - V_c)^2} = \frac{9\varepsilon_0 A}{8d^2}. \tag{6}$$

If equation (6) holds, the expression on the left-hand side should also be constant for different air pressures with the same gap distance. Figure 5 shows the measured curves of EHD force *versus* $(V_a - V_c)^2/d^2$. It shows that equation (6) is not fully satisfied, but the EHD force increases with $(V_a - V_c)^2/d^2$ increasing. The same result was also observed in Ref. [17]. Therefore, the accuracy of Eq. (1) at low air pressures is debatable.

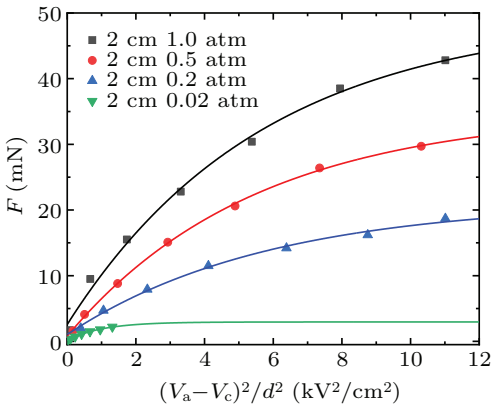


Fig. 5. EHD forces *versus* $(V_a - V_c)^2/d^2$ at different pressures.

3.3. Analysis by drift-diffusion model

To investigate more in depth the EHD forces at low pressures, here we use the drift-diffusion model developed by Morrow.[19] The drift-diffusion model has been validated.[20] It provides detailed insights into corona discharge and EHD force. The model includes the Navier–Stokes equation for airflow, Poisson's equation for electrostatic potential, and charge continuity equation as follows:

$$\nabla^2 V = -\frac{\sum_i q_i N_i}{\varepsilon}, \tag{7}$$

$$\frac{\partial(q_i N_i)}{\partial t} + \nabla\cdot\boldsymbol{J}_i = q(S_i - R_i), \tag{8}$$

$$\boldsymbol{J}_i = q_i N_i(\mu_i \boldsymbol{E} + \boldsymbol{v}) - q_i D_i \nabla N_i, \tag{9}$$

$$\frac{\partial \boldsymbol{v}}{\partial t} + (\boldsymbol{v}\cdot\nabla)\boldsymbol{v} = \nu\Delta\boldsymbol{v} - \nabla P + \boldsymbol{F}/\rho_{\text{air}}, \tag{10}$$

where N_i is the number density of type I ions or electrons, q_i is their charge, S_i is their production rate, R_i is the loss rate

due to recombination and collision, $\boldsymbol{\upsilon}$ is the flow velocity, is the current density, D_i is the diffusion coefficient of ions, μ_i is the electric mobility of ions, v is the kinematic viscosity, $\boldsymbol{F}$ is the EHD force, and ρ_{air} is the density of the atmosphere. The EHD force is calculated from

$$\boldsymbol{F} = \sum_i q_i N_i \boldsymbol{E}. \tag{11}$$

Here, we have neglected the heat transfer process. Equations (8) and (9) describe the generation, drift, and diffusion of ions and electrons during a corona discharge. The production rate or loss rate of ions can be calculated by the cross-section area of the chemical reactions during air discharge.[21] Equation (10) describes the effect of the EHD force on airflow. We adopt a boundary condition of anode and cathode expressed by the following coefficients[22]

$$\begin{cases} \alpha_i N_i + \beta \partial_n N_i = \kappa_i, \\ \alpha_i = q_i \mu_i E_{\text{on}}, \quad \beta = 0, \\ \kappa_i = q_i \mu_i E_{\text{on}} N_{\text{ref}}^{\text{i}} \exp\left(\dfrac{E_{\text{n}} - E_{\text{on}}}{E_{\text{ref}}}\right), \end{cases} \tag{12}$$

where E_{n} is the normal electric field at the anode, $N_{\text{ref}}^{\text{i}}$ is the reference density for type I ions, E_{ref} is a reference electric field strength, and E_{on} is the onset electric field to trigger a corona discharge, it changes with air pressure. A simple relation at constant temperature is

$$E_{\text{n}} = E_{\text{n0}} \frac{P}{P_0}, \tag{13}$$

where E_{n0} is the onset electric field at the standard air pressure P_0, and P is the working pressure for E_{n}. We use Eqs. (7)–(12) to calculate corona discharge characteristics in the wire-to-cylinder cell used in the experiments. We consider ions O_2^+ and N_2^+ because they are present in most air molecules.

According to the ion or electron behavior in a corona discharge, the space around electrodes can be divided into ionization region and drift region. The ionization region is around the anode surface. Kaptsov's hypothesis states that the free charge emitted by a steady-state corona for voltages above the inception voltage causes the anode to be shielded, which results in the clamping of the anode electric field at the onset value.[23] This region is called the ionization region. Its radius r_i can be calculated by using the bias voltage V_{a} and air breakdown electric field strength E_{on}. When the ions leave the ionization region, they, driven by the electric field, move to the cathode. The region where the ions drift and diffuse is the drift region. However, not all the ions or electrons can contribute to the EHD force, for some of them escape to the wall and cause the leakage current. Besides, the electric field has multiple directions when the wall is grounded as shown in Fig. 6.

In Fig. 6, the electric field E_x is generated in two opposite directions. One direction follows the ionic wind flowing rightward, and the strongest electric field exists between the anode and the cathode. On the left side of the anode, the electric field pushes the ions leftward, generating a counter-direction force that reduces the EHD force effect of the cell. As a result, not all the ions of the discharging current can contribute to EHD force, as indicated in Eq. (1).

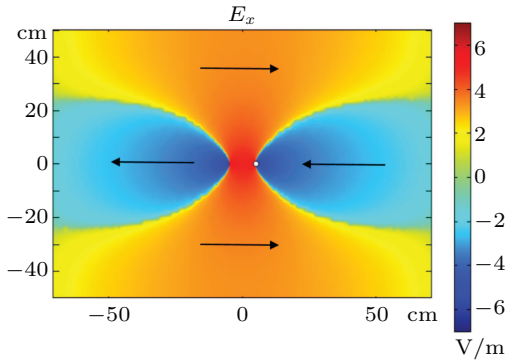


Fig. 6. Distribution of two-dimensional electric field E_x in wire-to-cylinder cell.

Most of ionization and recombination processes take place in the ionization region, so we can neglect the production rate and loss rate in the drift region in Eq. (8). We assume that the ratio of O_2^+ to N_2^+ follows their molecular proportion in the air. The Dirichlet boundary condition on the anode is

$$\begin{cases} V = V_{\text{a}}, \\ N_{\text{i}} = N_{\text{ref}}^{\text{i}} \exp\left(\frac{E_{\text{n}} - E_{\text{on}}}{E_{\text{ref}}}\right), \\ \upsilon = 0. \end{cases} \tag{14}$$

The electric potential V, ion density N_{i}, and flow velocity $\boldsymbol{\upsilon}$ are all set to zero on the wall and cathode, for they are grounded. However, there is a difference between the airflows on the inlet and outlet wall where we use the Neumann boundary condition

$$\frac{\partial V}{\partial n} = \frac{\partial N_{\text{i}}}{\partial n} = \frac{\partial \upsilon}{\partial n} = 0. \tag{15}$$

At the initial stage, no ions move in the drift region. The initial ion current density $\boldsymbol{J}_i$ and flow velocity $\boldsymbol{\upsilon}$ are both set to zero in the drift region. The EHD force is also zero. There exists only the electric field between the anode and the cathode. When the ions leave the anode and drift to the cathode, the EHD force grows up, resulting in an ionic wind. It reaches a balance when there appears a steady distribution of the ion density.

We solve these equations by using the COMSOL Multiphysics software. The electrostatic module, transport of diluted species module and the laminar flow module are used. The model is solved by using the finite element method in the software. In the simulation, the mobility for O_2^+ is 2.47×10^{-4} $\text{m}^2\cdot\text{V}^{-1}\cdot\text{s}^{-1}$, and 2.04×10^{-4} $\text{m}^2\cdot\text{V}^{-1}\cdot\text{s}^{-1}$ for N_2^+. Their diffusion coefficients conform to the Einstein's relation. The total reference ion density on the anode is 1×10^{14} m^{-3} and the onset electric field is 2.88×10^6 V/m. The reference electric field is 10^7 V/m. We should notice that all these values

are at 1.0 atm. When the air pressure drops, the ion mobility and onset electric field change at the same time. They can be calculated by using the relations in Ref. [16]. A validation example for the model is shown in Fig. 7. The experimental data are cited from Ref. [7].

We analyze the charge density distributions for a two-dimensional EHD cell at different pressures. The results are shown in Fig. 8. The drift and diffusion area of ions expand as the air pressure drops. However, the electric field distribution remains unchanged as shown in Fig. 6. As a result, the proportion of ions that drift or diffuse toward the left direction of the anode substantially increases as shown in Fig. 9. By integrating the two opposite directions of EHD force, we can define F_{de} for the left direction EHD force and F_{ac} for the right direction. Figure 10 shows the variation of their ratio with air pressure.

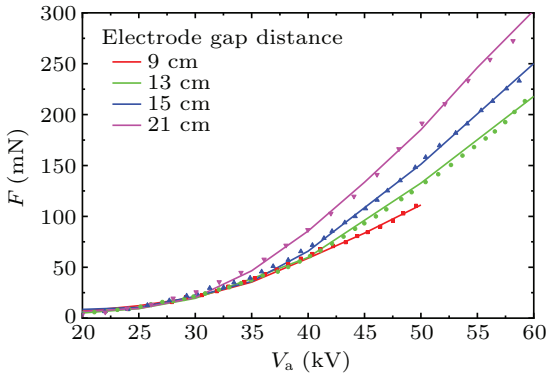


Fig. 7. Comparison between experimental results and simulation results, with lines representing simulation results and symbols denoting experiment results cited from Ref. [7].

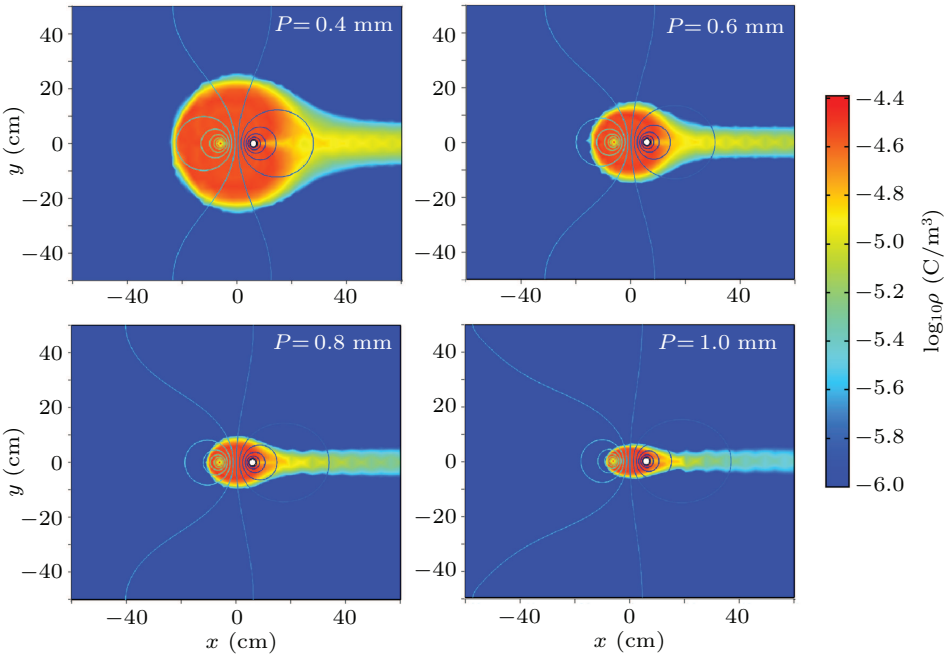


Fig. 8. Charge density distributions in thrust cell at different pressures, bias voltage of 20 kV, and electrode gap of 10 cm, with lines denoting electric potential contours.

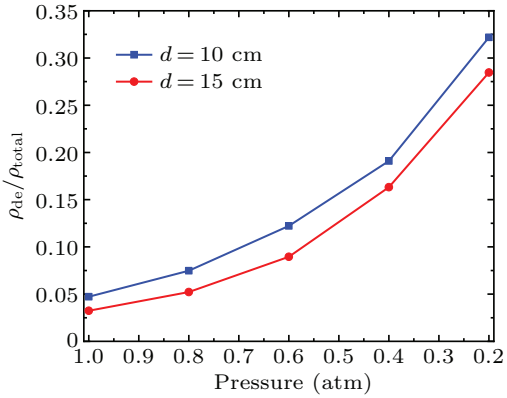


Fig. 9. Proportions of ions on left side of anode at different pressures and bias voltage of 20 kV for electrode gaps of 10 cm and 15 cm.

Figure 10 shows that the ratio F_{de}/F_{ac} increases with pressure lowering. The growth rate is different from that in Fig. 8 due to the irregular distribution of the electric field. Figures 9 and 10 suggest that when the air pressure drops, the counter-direction EHD force grows faster, thereby undermining the total thrust effect of the cell. The thrust efficiency of the EHD cell can be measured from the thrust-to-power ratio as follows:[23]

$$\lambda = \frac{F}{S} = \frac{F}{IV_a}, \tag{16}$$

where S is the supplied power. By adding it into the counter-direction EHD force, we can evaluate the thrust-to-power ratios for different air pressures. For comparison, we use the experimental results from Ref. [17] at constant power, and the theoretical predictions by previous theory under both high-field and low-field limits. The results are shown in Fig. 11. The average ion mobility used here is 1.67×10^{-4} m^2/(V/s).[24]

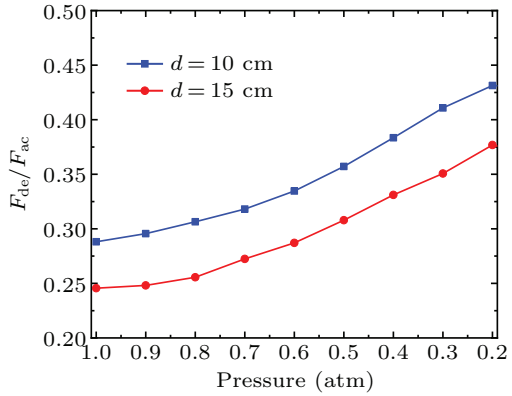


Fig. 10. Curves of ratio F_{de}/F_{ac} *versus* pressure for electrode gaps of 10 cm and 15 cm.

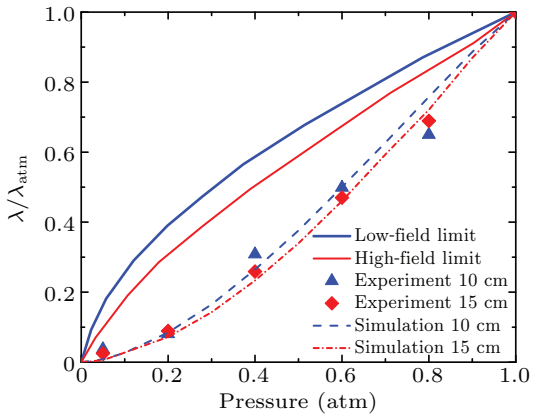


Fig. 11. Theoretical and experimental results of normalized thrust-to-power ratio *versus* air pressure at a given power. The dashed lines are simulation results obtained by using drift-diffusion model. The symbols show the experimental results cited from Ref. [17] at a constant power.

According to the previous estimation, the loss of λ is about 29% by the low-field limit and about 40% by the high-field limit when the air pressure drops from 1 atm to 0.6 atm. However, the experimental results are 50% loss for 10-cm gap and 53% loss for 15-cm gap. With the drift-diffusion model, the rate updates to 51% for 10-cm gap and 54% loss for 15-cm gap, which gives a better estimation. Thus the counter-direction EHD force is also an important factor when the air pressure drops.

4. Conclusions and perspectives

In this work, we investigated the effect of air pressure on the EHD force of a wire-to-cylinder cell. The EHD force and corona discharge current were measured at different air pressures and electrode gap distances. Experimental result shows that increasing the corona discharge current does not lead to a proportional growth in the EHD force at low air pressures. Their linear dependence breaks down when the air pressure drops. We used the drift-diffusion model to analyze the reason and found that there might exist a counter-direction EHD force to undermine the total EHD force in the cell. The simulation result showed that the ion drift region expands and the proportion of ions accelerated in the opposite direction is increased when the air pressure drops. By counting in this effect, a more correct estimation of the thrust-to-power ratio for low air pressures can be obtained.

A corona discharge under high voltage is a complicated physical and chemical processes. The types of ions to be considered in the model and the variation of ion mobility with air pressure remain to be further investigated. Although we showed that there is a counter-direction EHD force on the left side of the anode, further experimental proof, such as particle image velocimetry of the cell, is necessary. In real conditions, there is no grounded wall, and electrodes are electrically isolated. Its practical application should be further studied.

Acknowledgement

Project supported by the National Natural Science Foundation of China (Grant No. 51877111).

References

[1] Robinson M 1961 *Trans. Am. Inst. Electr. Eng., Part I* **80** 143
[2] Ye J C, Li J, Chen X H, Huang S M and OuYang W 2019 *Chin. Phys. B* **28** 095202
[3] Yamamoto T and Velkoff H R 1981 *J. Fluid Mech.* **108** 1
[4] Hohman M M, Shin M, Rutledge G and Brenner M P 2001 *Phys. Fluids* **13** 2201
[5] Bian D L, Wu Y, Jia M, Long C B and Jiao S B 2017 *Chin. Phys. B* **26** 084703
[6] Moreau E, Benard N, Lan-Sun-Luk J D and Chabriat J P 2013 *J. Phys. D: Appl. Phys.* **46** 475204
[7] Masuyama K and Barrett S R H 2013 *Proc. R. Soc. A* **469** 20120623
[8] Xu H F, He Y, Strobel K L, Gilmore C K, Kelley S P, Hennick C C, Sebastian T, Woolston M R, Perreault D J and Barrett S R H 2018 *Nature* **563** 532
[9] Zhang G W, Yang J K and Lin X H 2021 *Chin. Phys. B* **30** 014701
[10] Moreau E, Benard N, Alicalapa F and Douyere A 2015 *J. Electrost.* **76** 194
[11] Zhang T K, Zhang Y, Ji Q Z, Li B and Ouyang J T 2019 *Chin. Phys. B* **28** 075202
[12] Wynsberghe E and Turak A 2016 *Acta Astronaut.* **128** 616
[13] Guerra-Garcia C, Nguyen N C, Mouratidis T and Martinez-Sanchez M 2020 *J. Geophys. Res.: Atmos.* **125** e2020JD032908
[14] Monrolin N, Plouraboué F and Praud O 2017 *AIAA J.* **55** 4296
[15] Marčiulionis P 2020 *J. Electrost.* **105** 103446
[16] Gilmore C K and Barrett S R H 2018 *AIAA J.* **56** 1105
[17] Khomich V Y, Malanichev V E and Rebrov I E 2021 *Acta Astronaut.* **180** 141
[18] Jignesh S and Subrata R 2013 *Appl. Phys. Lett.* **102** 112908
[19] Morrow R 1985 *Phys. Rev. A* **32** 1799
[20] Ignjatovic M and Cvetic J 2021 *Int. J. Elec. Power* **129** 106815
[21] Hagelaar G J M and Pitchford L C 2005 *Plasma Sources Sci. Technol.* **14** 722
[22] Cagnoni D, Agostini F, Christen T, Parolini N, Stevanović I and Falco C 2013 *J. Appl. Phys.* **114** 233301
[23] Gilmore C K and Barrett S R H 2015 *Proc. R. Soc. A* **471** 20140912
[24] Yi Y, Chen Z Y and Wang L M 2020 *IEEE Access* **8** 150142